Plasmonic propagation modes of a structured two-dimensional conducting interface

2008 J. Opt. A: Pure Appl. Opt. 10 025202

(http://iopscience.iop.org/1464-4258/10/2/025202)

J. Opt. A: Pure Appl. Opt. **10** (2008) 025202 (7pp) doi:10.1088/1464-4258/10/02/025202

Plasmonic propagation modes of a structured two-dimensional conducting interface

Hesam Zandi[1], Sina Khorasani[1], Amir Hosseini[1], Khashayar Mehrany[1], Bizhan Rashidian[1] and Ali Adibi[2]

[1] School of Electrical Engineering, Sharif University of Technology, PO Box 11365-9363, Tehran, Iran
[2] School of Electrical and Computer Engineering, Georgia Institute of Technology, Atlanta, GA 30332-0250, USA

E-mail: khorasani@sina.sharif.edu and adibi@ece.gatech.edu

Received 18 November 2007, accepted for publication 20 December 2007
Published 11 January 2008
Online at stacks.iop.org/JOptA/10/025202

Abstract
In this paper, we present a detailed analysis of a two-dimensional lossless and non-dispersive structured conducting interface, which is approximated by a two-dimensional ideal one-component plasma-like conducting sheet enclosed by two isotropic dielectrics. We present a Green's function formalism to analyze the propagation of surface plasmons and find new expressions. We also present analytical extensions of the approach to include loss, and discuss the results and applications of the theory. We study the symmetry properties of eigenmodes and show that the symmetries of the eigenmodes at high-symmetry points of the Brillouin zone are similar to those of the E-polarization eigenmodes of a two-dimensional square-lattice photonic crystal.

Keywords: optics at surfaces, surface plasmons, photonic crystals, conducting interfaces

(Some figures in this article are in colour only in the electronic version)

1. Introduction

In recent years, the propagation of plasmons on the surface of metallic nanostructures [1] has attracted much attention, particularly due to the anomalous diffraction and dispersion properties. It is quite expected that plasmonics would prevail in the field of nanotechnology, where optical communications need sub-wavelength feature sizes [2]. Metallic nanostructures have found applications in sub-wavelength imaging well beyond the classical diffraction limit [3]. Maier *et al* [4] have considered the propagation and focusing of terahertz surface plasmon polaritons on periodically corrugated metal wires. They have shown that the corresponding dispersion relation can be tailored by corrugating the metal's surface with a periodic array of radial grooves, and hence highly localized surface plasmon polaritons can be sustained in the terahertz region. Khurgin has discussed the possibility of optical insulating action using surface plasmon polaritons with possible applications to short nanoplasmonic guides with low insertion loss [5]. Novel applications of plasmons have been further demonstrated, such as the enhancement of luminescence [6, 7] and spontaneous emission efficiency [8], as well as laser cooling of solids [9]. An extensive review of the literature on the theory of surface plasmons and surface-plasmon polaritons has recently been published [10], to which the reader is referred for more details.

A recent analytical study by Wuenschell and Kim [11] has considered the dynamic interplay among plasmon polarization charges, electromagnetic fields, and energy flow in the metal/dielectric interface and metal nanoslit structure, and revealed that a vortex-like circulation of energy is an intrinsic feature of plasmons in such structures. Lan and Chern [12] studied plasmons on perfectly conducting surfaces and obtained the dispersion of surface plasmon-like modes which occur on the surface of perfectly conducting structures numerically.

In this paper, we present a simple model for long-range plasmons [13, 14] on the surface of a thin highly conductive

film, which is assumed to be periodically patterned. We initially take a lossless and non-dispersive approximation for the conductive film and analytically obtain the governing equation of plasmons. To model the conductive film, we employ the concept of conducting interfaces published in our earlier papers [15–17]. This idea has proven to be extremely useful in modeling Krönig–Penney photonic crystals [16, 18, 19], and later independently by Schulkin *et al* [20]. We then employ a plane-wave expansion method to obtain the corresponding band structure of plasmons. Extensions to the case of a dispersive and lossy conducting sheet will also be discussed. The structure considered in this paper also models the plasmons of an anti-dot lattice obtained by patterning of the two-dimensional electron gas (2DEG) formed at the interface of semiconductor heterostructures [21]; such structures are believed to have applications in quantum computing [21].

As is generally known, the standard numerical methods such as plane-wave expansion fail in the case of dispersion [22]. In order to resolve this difficulty, various schemes have been proposed [23–25]. However, we present a formalism based on which we are able to show that the full band structure of the dispersive medium of interest can be obtained without using numerical methods, and show that a band structure survives in the lossy part of the angular frequency. As a result, we conclude that the absorption spectrum of the structure would no longer extend over the whole frequency range. But certain allowed frequency absorption bands and forbidden frequency absorption bands are expected, quite similar to the band structure of a normal photonic crystal. Hence, a lossy metallic thin film can be arbitrarily trimmed using periodic patterning to absorb the electromagnetic power in certain windows of wavelength.

The organization of the paper is as follows. In section 2 we present our mathematical model and discuss the lossless non-dispersive and lossy dispersive cases, respectively. Then in section 3 we present several examples in the same two categories. In each case the structure of the frequency and absorption bands as well as the eigenmodes will be considered and discussed. Finally in section 4 we present our conclusions.

2. Mathematical model

In order to properly model the propagation of plasmons on the conducting sheet, we assume that a planar thin conductor lies along the interface of two isotropic dielectrics. Without loss of generality we take both the dielectrics to be air. If the thickness of the conductor film is much less than the wavelength, one can shrink the thickness even further towards zero, while increasing the conductivity to the same order. In the limit of infinitesimal thickness, the approximation of a conducting interface [15–20] applies. If the interface is characterized by the plane $z = 0$ we have

$$\sigma(\mathbf{r}) = c(\mathbf{r}_\parallel)\delta(z). \tag{1}$$

Here $\sigma(\mathbf{r})$ is the conductivity having the dimension of $(\Omega\ \mathrm{m})^{-1}$, and in general it is frequency dependent; $\delta(z)$ is the Dirac's delta, $\mathbf{r}_\parallel = x\hat{x} + y\hat{y}$, while $\mathbf{r} = x\hat{x} + y\hat{y} + z\hat{z}$. Also $c(\mathbf{r}_\parallel)$ describes the position-dependence of conductivity across the interface. Clearly,

$$\mathbf{J}(\mathbf{r}) = \sigma(\mathbf{r})\mathbf{E}(\mathbf{r}) \equiv \mathbf{J}(\mathbf{r}_\parallel), \tag{2}$$

in which $\mathbf{E}(\mathbf{r})$ and $\mathbf{J}(\mathbf{r})$ are respectively the electric field and current density vector fields.

We assume a periodic inclusion of air holes forming a two-dimensional plasmonic lattice out of the dielectric. Hence,

$$c(\mathbf{r}_\parallel) = c(\mathbf{r}_\parallel + \mathbf{T}_{mn}), \tag{3}$$

where $\mathbf{T}_{mn} = m\mathbf{a} + n\mathbf{b}, \forall m, n \in \mathrm{Z}$, with $\mathbf{a} \equiv \mathbf{a}_\parallel$ and $\mathbf{b} \equiv \mathbf{b}_\parallel$ being the lattice basis vectors. Obviously, a consistent formulation requires that the unit cell has non-vanishing area, that is $A_{\mathrm{cell}} = \mathbf{a} \times \mathbf{b} \cdot \hat{z} \neq 0$.

Now the vector-potential formulation in the Coulomb gauge is simply given by [26]

$$\mathbf{A}(\mathbf{r}) = \int G(\mathbf{r}, \mathbf{r}')\mathbf{J}(\mathbf{r}')\,\mathrm{d}^3 r', \tag{4}$$

where the integration is taken over all space and $G(\mathbf{r}, \mathbf{r}')$ is the Green's function of the vector potential given by

$$G(\mathbf{r}, \mathbf{r}') = \frac{\mu_0}{4\pi}\frac{1}{|\mathbf{r} - \mathbf{r}'|}. \tag{5}$$

Here, μ_0 is the permeability of vacuum. Then we have $\mathbf{E}(\mathbf{r}) = -\frac{\partial}{\partial t}\mathbf{A}(\mathbf{r})$. Hence for single-frequency harmonic excitations we get

$$\mathbf{A}(\mathbf{r}) = -\frac{\mathrm{j}\omega\mu_0}{4\pi}\int \frac{c(\mathbf{r}'_\parallel; \omega)}{|\mathbf{r} - \mathbf{r}'_\parallel|}\mathbf{A}(\mathbf{r}'_\parallel)\,\mathrm{d}^2 r'_\parallel. \tag{6}$$

In order to solve (6) we consider two cases: the lossless non-dispersive case, $\sigma(\mathbf{r}; \omega) \equiv \mathrm{j}\sigma_i(\mathbf{r})$, and the lossy dispersive case, $\sigma(\mathbf{r}; \omega) \equiv \sigma_r(\mathbf{r}; \omega) + \mathrm{j}\sigma_i(\mathbf{r}; \omega)$.

2.1. Lossless non-dispersive case

Equation (6) for the case of a lossless non-dispersive conductivity reads

$$\mathbf{A}(\mathbf{r}) = \frac{\omega\mu_0}{4\pi}\int \frac{c_i(\mathbf{r}'_\parallel)}{|\mathbf{r} - \mathbf{r}'_\parallel|}\mathbf{A}(\mathbf{r}'_\parallel)\,\mathrm{d}^2 r'_\parallel, \tag{7}$$

which can further be simplified to

$$\mathbf{A}(\mathbf{r}_\parallel) = \frac{\omega\mu_0}{4\pi}\int \frac{c_i(\mathbf{r}'_\parallel)}{|\mathbf{r}_\parallel - \mathbf{r}'_\parallel|}\mathbf{A}(\mathbf{r}'_\parallel)\,\mathrm{d}^2 r'_\parallel \tag{8}$$

on the $z = 0$ plane. Notice that from now on, the parallel subscript will not be shown for the sake of simplicity, unless pointed out. Now due to the periodicity we have the expansion

$$c_i(\mathbf{r}) = \sum_{m,n=-\infty}^{\infty} c_{i,mn}\mathrm{e}^{-\mathrm{j}\mathbf{G}_{mn}\cdot\mathbf{r}} \equiv \sum_{\mathbf{G}} c_{i\mathbf{G}}\mathrm{e}^{-\mathrm{j}\mathbf{G}\cdot\mathbf{r}}. \tag{9}$$

Here, $\mathbf{G}_{mn} = m\mathbf{a}^* + n\mathbf{b}^*$ with $\mathbf{a}^*$ and $\mathbf{b}^*$ being reciprocal lattice vectors, given by

$$\mathbf{a}^* = 2\pi\frac{\mathbf{b} \times \hat{z}}{A_{\mathrm{cell}}} \tag{10}$$

$$\mathbf{b}^* = 2\pi \frac{\hat{z} \times \mathbf{a}}{A_{\text{cell}}}. \tag{11}$$

It is easy to observe that for the area of the Brillouin zone, we have $A_{\text{BZ}} = \frac{4\pi^2}{A_{\text{cell}}}$, and therefore the Bloch–Floquet solutions of (9) are in the form [22]

$$\mathbf{A}(\mathbf{r}) = \mathrm{e}^{-\mathrm{j}\mathbf{k}\cdot\mathbf{r}} \sum_{\mathbf{G}} \mathbf{A}_{\mathbf{G}} \mathrm{e}^{-\mathrm{j}\mathbf{G}\cdot\mathbf{r}} = \sum_{\mathbf{G}} \mathbf{A}_{\mathbf{G}} \mathrm{e}^{-\mathrm{j}(\mathbf{k}+\mathbf{G})\cdot\mathbf{r}}, \tag{12}$$

with $\mathbf{k} \equiv k_x\hat{x} + k_y\hat{y}$ being the two-dimensional Bloch wavevector. Plugging (9) and (12) into (8) we get

$$\sum_{\mathbf{G}} \mathbf{A}_{\mathbf{G}} \mathrm{e}^{-\mathrm{j}(\mathbf{k}+\mathbf{G})\cdot\mathbf{r}} \tag{13}$$

$$= \frac{\omega\mu_0}{4\pi} \sum_{\mathbf{G}',\mathbf{G}''} c_{i\mathbf{G}'} \mathbf{A}_{\mathbf{G}''} \int \frac{\mathrm{e}^{-\mathrm{j}(\mathbf{k}+\mathbf{G}'+\mathbf{G}'')\cdot\mathbf{r}'}}{|\mathbf{r}-\mathbf{r}'|} \mathrm{d}^2 r', \tag{14}$$

or

$$\sum_{\mathbf{G}} \mathbf{A}_{\mathbf{G}} \mathrm{e}^{-\mathrm{j}(\mathbf{k}+\mathbf{G})\cdot\mathbf{r}} = \frac{\omega\mu_0}{4\pi} \times \sum_{\mathbf{G}',\mathbf{G}''} c_{i\mathbf{G}'} \mathbf{A}_{\mathbf{G}''} \mathrm{e}^{-\mathrm{j}(\mathbf{k}+\mathbf{G}'+\mathbf{G}'')\cdot\mathbf{r}} \int \frac{\mathrm{e}^{\mathrm{j}(\mathbf{k}+\mathbf{G}'+\mathbf{G}'')\cdot(\mathbf{r}-\mathbf{r}')}}{|\mathbf{r}-\mathbf{r}'|} \mathrm{d}^2 r'. \tag{15}$$

Using the definitions $\mathbf{h} = \mathbf{G}' + \mathbf{G}'' + \mathbf{k}$ and $\mathbf{s} = \mathbf{r} - \mathbf{r}'$, the integrand in (15) turns into the form of a two-dimensional Fourier transform, which simplifies as

$$\int \frac{\mathrm{e}^{\mathrm{j}\mathbf{h}\cdot\mathbf{s}}}{s} \mathrm{d}^2 s = \frac{2\pi}{h}. \tag{16}$$

Here, $h = |\mathbf{h}|$ and $s = |\mathbf{s}|$. Therefore, equation (15) can be rewritten as

$$\sum_{\mathbf{G}} \mathbf{A}_{\mathbf{G}} \mathrm{e}^{-\mathrm{j}\mathbf{G}\cdot\mathbf{r}} = \frac{\omega\mu_0}{2} \sum_{\mathbf{G}',\mathbf{G}''} \frac{c_{i\mathbf{G}'} \mathbf{A}_{\mathbf{G}''} \mathrm{e}^{-\mathrm{j}(\mathbf{G}'+\mathbf{G}'')\cdot\mathbf{r}}}{|\mathbf{k}+\mathbf{G}'+\mathbf{G}''|} \tag{17}$$

$$= \frac{\omega\mu_0}{2} \sum_{\mathbf{G},\mathbf{G}'} \frac{c_{i\mathbf{G}-\mathbf{G}'} \mathbf{A}_{\mathbf{G}'} \mathrm{e}^{-\mathrm{j}\mathbf{G}\cdot\mathbf{r}}}{|\mathbf{k}+\mathbf{G}|}. \tag{18}$$

This last expression, however, translates into the matrix equation

$$\mathbf{A}_{\mathbf{G}} = \frac{\omega\mu_0}{2} \sum_{\mathbf{G}'} \frac{c_{i\mathbf{G}-\mathbf{G}'}}{|\mathbf{k}+\mathbf{G}|} \mathbf{A}_{\mathbf{G}'}. \tag{19}$$

Finally, by defining

$$\varpi(\mathbf{k}) = \frac{\omega\mu_0}{2}, \tag{20}$$

$$\{\mathbf{A}\} = \{\mathbf{A}_{\mathbf{G}}\}, \tag{21}$$

$$[\mathbf{D}(\mathbf{k})] \equiv [\mathbf{D}_{\mathbf{G},\mathbf{G}'(\mathbf{k})}] = \left[\frac{c_{i\mathbf{G}-\mathbf{G}'}}{|\mathbf{k}+\mathbf{G}|}\right], \tag{22}$$

we get

$$\{\mathbf{A}\} = \varpi(\mathbf{k})[\mathbf{D}(\mathbf{k})]\{\mathbf{A}\}, \tag{23}$$

which reads

$$\varpi^{-1}(\mathbf{k}) = \mathrm{eig}\{[\mathbf{D}(\mathbf{k})]\}. \tag{24}$$

Hence, the normalized band structure $\varpi(\mathbf{k})$ can be found by the negative of the inverse eigenvalues of the matrix $[\mathbf{D}(\mathbf{k})]$. Upon computing the eigenvectors from the above, one can easily recover the complete eigenfunctions in three-dimensional space using (7) as

$$\mathbf{A}_{\mathbf{k}}(\mathbf{r}) = \frac{\varpi(\mathbf{k})}{2\pi} \sum_{\mathbf{G},\mathbf{G}'} c_{i\mathbf{G}} A_{\mathbf{G}'} \int \frac{\mathrm{e}^{-\mathrm{j}(\mathbf{k}+\mathbf{G}+\mathbf{G}')\cdot\mathbf{r}'_{\parallel}}}{|\mathbf{r}-\mathbf{r}'_{\parallel}|} \mathrm{d}^2 r'_{\parallel}, \tag{25}$$

in which $\mathbf{r}$ denotes again the three-dimensional position vector. This, however, can be further simplified similarly to (15), using the Fourier transform

$$\int \frac{\mathrm{e}^{\mathrm{j}\mathbf{h}\cdot\mathbf{s}}}{\sqrt{s^2+z^2}} \mathrm{d}^2 s = \frac{2\pi}{h} \exp(-2\pi h|z|). \tag{26}$$

This is equivalent to

$$\mathbf{A}_{\mathbf{k}}(\mathbf{r}) = \varpi(\mathbf{k}) \sum_{\mathbf{G},\mathbf{G}'} c_{i\mathbf{G}-\mathbf{G}'} A_{\mathbf{G}'} \frac{\mathrm{e}^{-2\pi|\mathbf{k}+\mathbf{G}||z| - \mathrm{j}(\mathbf{k}+\mathbf{G})\cdot\mathbf{r}_{\parallel}}}{|\mathbf{k}+\mathbf{G}|}. \tag{27}$$

It is worth mentioning that the last equation for the trivial case of $c_i(\mathbf{r}) = c_0$ relaxes to

$$\varpi(\mathbf{k}) = \frac{k}{c_0}, \tag{28}$$

$$\mathbf{A}_{\mathbf{k}}(\mathbf{r}) = A_0 \mathrm{e}^{-2\pi k|z| - \mathrm{j}\mathbf{k}\cdot\mathbf{r}_{\parallel}}, \tag{29}$$

which characterizes a non-dispersive constant phase-velocity plasmon with an exponentially decaying profile across the z-axis, having an amplitude A_0. By defining the three-dimensional wavevector $\mathbf{K} = \mathbf{k} - \mathrm{j}2\pi k\hat{z}$ and the symmetrized position vector $\tilde{\mathbf{r}} = \mathbf{r}_{\parallel} + |z|\hat{z}$, the last equation can be rewritten as

$$\mathbf{A}_{\mathbf{K}}(\mathbf{r}) = A_0 \mathrm{e}^{-\mathrm{j}\mathbf{K}\cdot\tilde{\mathbf{r}}}. \tag{30}$$

2.2. Lossy dispersive case

In case of a frequency-dependent conductivity with non-vanishing real part, (19) changes into

$$\mathbf{A}_{\mathbf{G}} = -\mathrm{j}\frac{\omega\mu_0}{2} \sum_{\mathbf{G}'} \frac{c_{r\mathbf{G}-\mathbf{G}'}(\omega) + \mathrm{j}c_{i\mathbf{G}-\mathbf{G}'}(\omega)}{|\mathbf{k}+\mathbf{G}|} \mathbf{A}_{\mathbf{G}'}. \tag{31}$$

In particular, for a Drude-type conductivity and homogeneous constituents we have

$$c_{\mathbf{G}}(\omega) = \frac{\omega_{\mathrm{p}}^2 \tau \epsilon_0}{1 + \mathrm{j}\omega\tau} f_{\mathbf{G}}, \tag{32}$$

where τ is the relaxation time, ω_{p} is the plasma frequency, ϵ_0 is the permittivity of vacuum, and $f_{\mathbf{G}}$ are the dimensionless spatial harmonic coefficients of the shape function, describing the two-dimensional geometry of the conducting sheet. Hence, we have

$$c_{r\mathbf{G}}(\omega) = \frac{\omega_{\mathrm{p}}^2 \tau \epsilon_0}{1 + (\omega\tau)^2} f_{\mathbf{G}}, \tag{33}$$

$$c_{i\mathbf{G}}(\omega) = -\frac{\omega_{\mathrm{p}}^2 \tau^2 \epsilon_0 \omega}{1 + (\omega\tau)^2} f_{\mathbf{G}}. \tag{34}$$

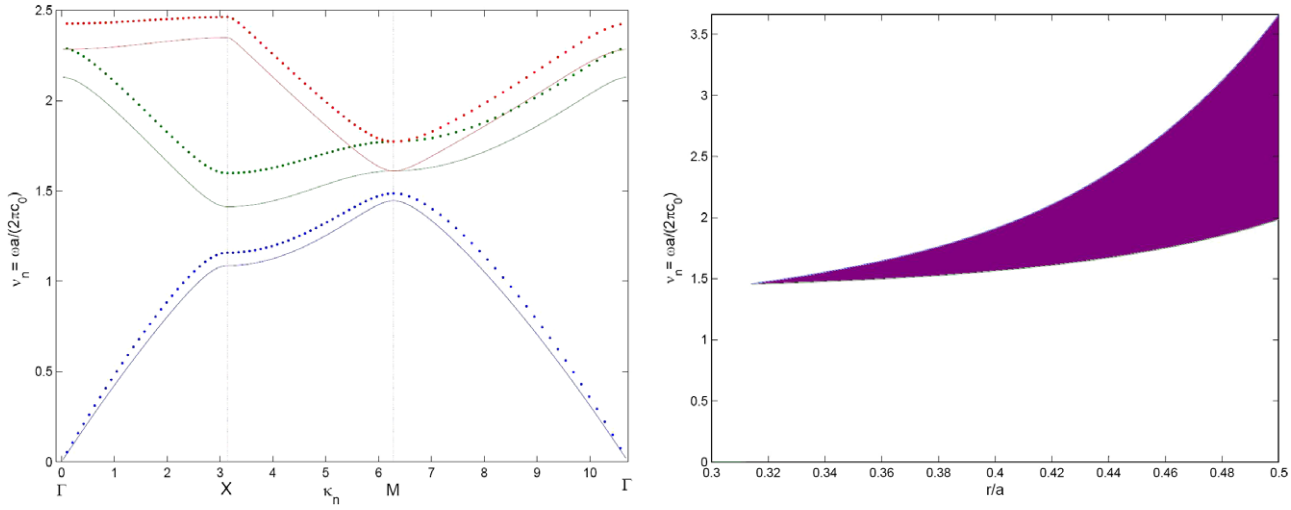

Figure 1. Left: band structure of a lossless and non-dispersive structure with the unpatterned conductivity $\sigma(\mathbf{r}) = -\mathrm{j}\delta(z)$, $\frac{r}{a} = 0.30$ (solid curve) and $\frac{r}{a} = 0.35$. There is no frequency gap for the first case, while for the second case $\Delta\nu_n = 1.057 \times 10^{-1}$. Right: gap-map for the lossless non-dispersive structures with the same conductivity, showing that no first gap is expected for $\frac{r}{a} \leqslant 0.315$.

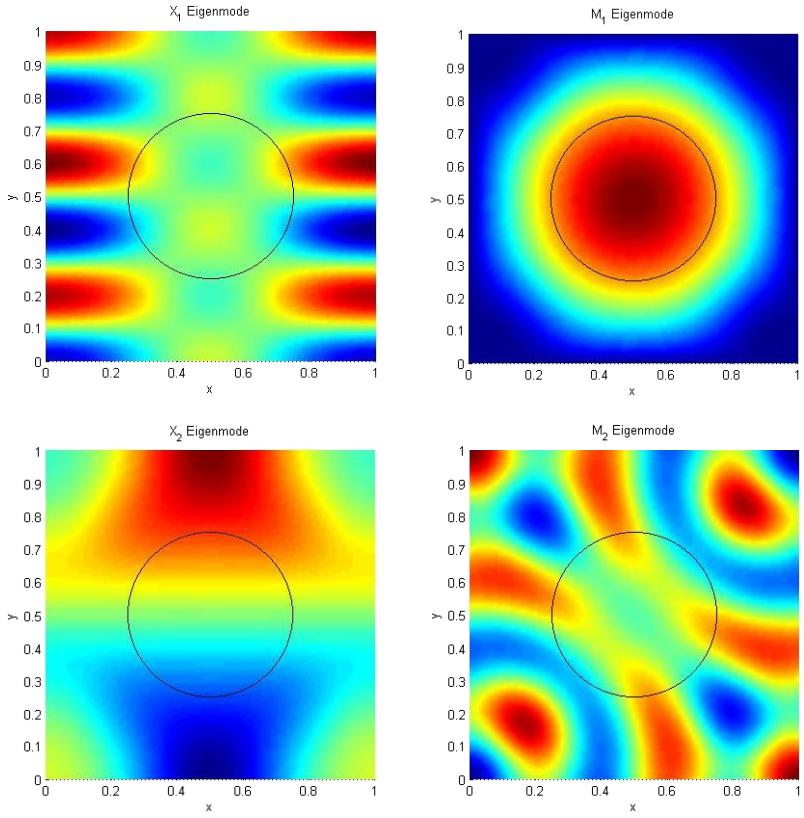

Figure 2. First and second eigenmodes for the lossless and non-dispersive case at various points in the corners of the reciprocal lattice $\mathbf{X} \equiv \frac{1}{2}\mathbf{a}^*$ and $\mathbf{M} \equiv \frac{1}{2}\mathbf{a}^* + \frac{1}{2}\mathbf{b}^*$. Here, the unpatterned conductivity is $\sigma(\mathbf{r}) = -\mathrm{j}\delta(z)$ and $\frac{r}{a} = 0.25$.

Plugging the latter into (31) and defining the normalized angular frequency $\Omega = \omega\tau$ and plasma wavenumber $K_\mathrm{p} = \omega_\mathrm{p}\sqrt{\epsilon_0\mu_0}$, we get

$$\mathbf{A}_\mathbf{G} = -\mathrm{j}\frac{\Omega K_\mathrm{p}^2}{2(1+\mathrm{j}\Omega)} \sum_{\mathbf{G}'} \frac{f_{\mathbf{G}-\mathbf{G}'}\mathbf{A}_{\mathbf{G}'}}{|\mathbf{k}+\mathbf{G}|}. \tag{35}$$

This equation can be rewritten as the eigenvalue equation

$$\Omega^{-1}(\mathbf{k}) = -\mathrm{j}\,\mathrm{eig}\left\{\mathbf{I} + \frac{K_\mathrm{p}^2}{2}[\mathbf{F}(\mathbf{k})]\right\}, \tag{36}$$

in which

$$[\mathbf{F}(\mathbf{k})] \equiv [\mathbf{F}_{\mathbf{G},\mathbf{G}'(\mathbf{k})}] = \left[\frac{f_{\mathbf{G}-\mathbf{G}'}}{|\mathbf{k}+\mathbf{G}|}\right]. \tag{37}$$

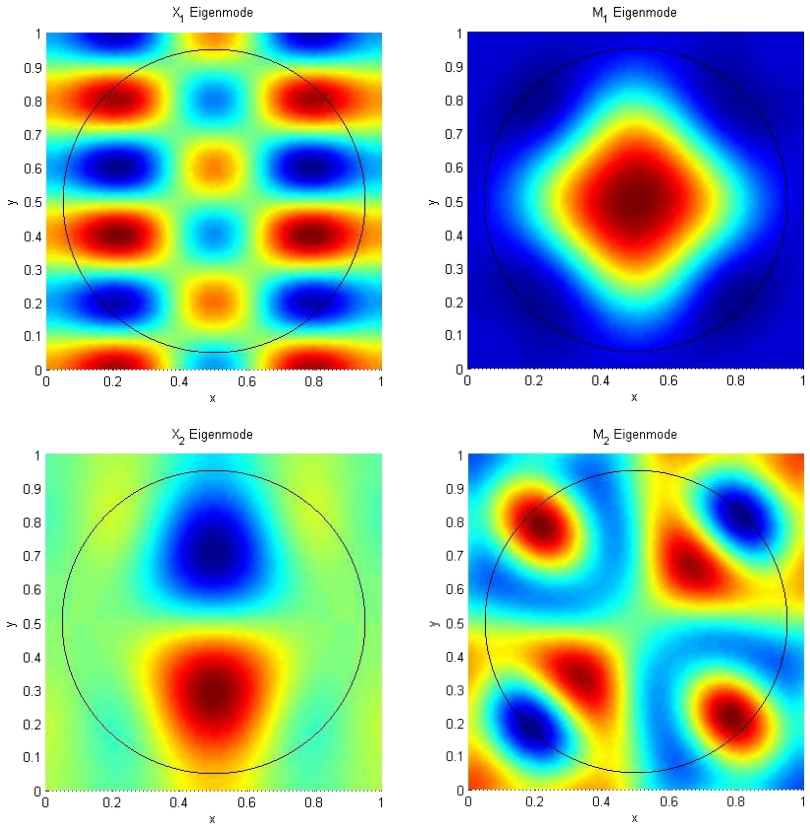

Figure 3. First and second eigenmodes for the lossless and non-dispersive case at various points in the corners of the reciprocal lattice $\mathbf{X} \equiv \frac{1}{2}\mathbf{a}^*$ and $\mathbf{M} \equiv \frac{1}{2}\mathbf{a}^* + \frac{1}{2}\mathbf{b}^*$. Here, the unpatterned conductivity is $\sigma(\mathbf{r}) = -\mathrm{j}\delta(z)$ and $\frac{r}{a} = 0.45$.

Notice that according to (36), all eigenvalues will be purely imaginary, since $[\mathbf{F}(\mathbf{k})]$ is purely real, and hence the matrix inside the braces is Hermitian with real eigenvalues. This proves our assertion that the in-plane attenuation exhibits a band-structure-like spectrum.

3. Results and discussions

In this section, the typical band structures, gap-maps, and eigenmodes of the solutions are calculated and plotted. First we study a lossless non-dispersive example and then move forward to a lossy and frequency-dependent one.

3.1. Lossless non-dispersive case

3.1.1. Band structure. In figure 1 the band structure and gap-map of a typical system are calculated and shown. In both cases, the conductivity of the unpatterned sheet is taken to be $-\mathrm{j}(\Omega\ \mathrm{m})^{-1}$, that is $\sigma(\mathbf{r}) = -\mathrm{j}\delta(z)$. For the sake of simplicity, we take the lattice constant also to be normalized to unity as $a = 1$. Also, the frequency $f = \frac{\omega}{2\pi}$ is normalized according to $\nu_n = \frac{\omega a}{2\pi c_0}$. These normalizations greatly help us to simplify the calculations. Here, the band structure is plotted for two different values of normalized radius: $\frac{r}{a} = 0.30$ and $\frac{r}{a} = 0.35$.

Both band structures look rather like the band structure of E-polarization in two-dimensional photonic crystals, although the governing equations are rather different. The first band starts from zero frequency and detaches from the Γ_0 point with non-zero group velocity. For $\frac{r}{a} = 0.30$, there is no gap, while for $\frac{r}{a} = 0.35$ a frequency gap of $\Delta\nu_n = 1.057 \times 10^{-1}$ opens around the normalized central frequency $\nu_n = 1.536$. This equals a gap-ratio of $\frac{\Delta\nu_n}{\nu_n} = 6.88\%$. Comparison to the second plot reveals that no first frequency gap could be expected for $\frac{r}{a} \leqslant 0.315$. This is in agreement with the band structures shown in figure 1.

3.1.2. Eigenmodes. We have plotted the first and second vector-potential eigenmodes $A_{z\mathbf{k}}$ on the high symmetry points $\mathbf{X} \equiv \frac{1}{2}\mathbf{a}^*$ and $\mathbf{M} \equiv \frac{1}{2}\mathbf{a}^* + \frac{1}{2}\mathbf{b}^*$ as shown in figures 2 and 3. Along with the origin $\Gamma \equiv 0$ of the reciprocal lattice, these two points constitute the corners of the irreducible Brillouin zone. Here, the same input parameters are used, while $\frac{r}{a} = 0.25$ and $\frac{r}{a} = 0.45$ for figures 2 and 3, respectively. These two values respectively correspond to two choices having gaps of zero and $\Delta\nu_n = 7.55 \times 10^{-1}$.

In both cases, the $\mathbf{M}_1$ and $\mathbf{M}_2$ points belong to the C_{4v} point group and display A_1 and B_2 symmetries, respectively, while the $\mathbf{X}_1$ and $\mathbf{X}_2$ points belong to the C_{2v} point group and have B_1 and A_1 symmetries, respectively. This is in remarkable agreement with the band structure of E-polarization in two-dimensional photonic crystals [22], while the governing equations are essentially different. As it can be easily seen, increasing the normalized radius $\frac{r}{a}$ from 0.25 to 0.45 has no effect on the symmetry of the eigenmodes. However, the maxima and minima have become more localized for the larger hole radius.

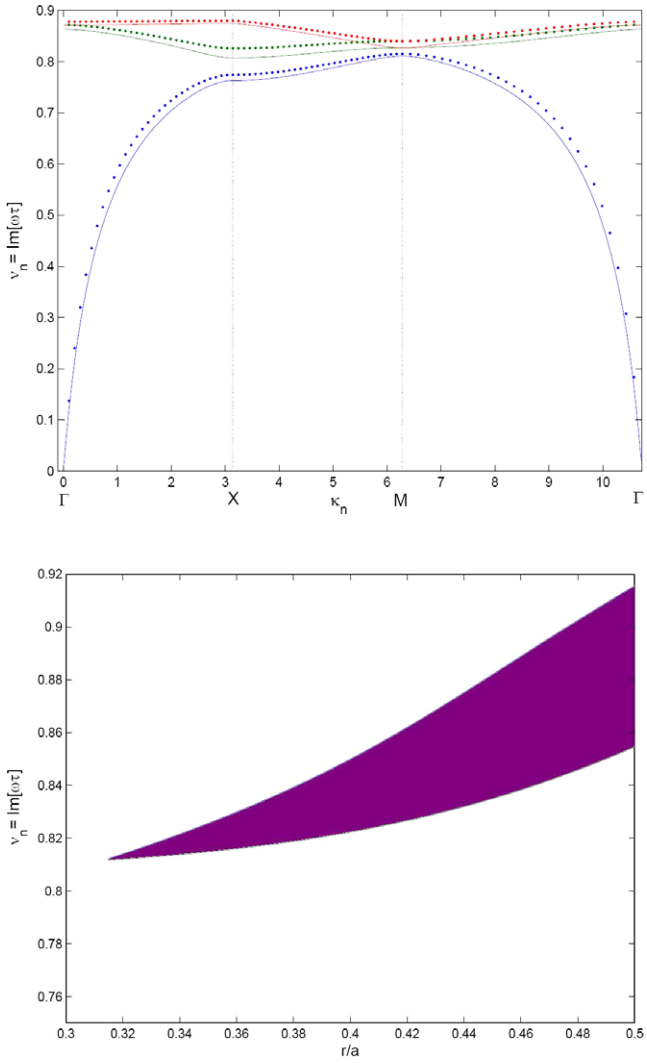

Figure 4. Top: band structure of a lossy and dispersive structure with $\Omega_\mathrm{p} = 10$, $\frac{r}{a} = 0.30$ (solid curve) and $\frac{r}{a} = 0.35$. There is no frequency gap for the first case, while for the second case $\Delta\nu_n = 1.017 \times 10^{-2}$. Bottom: gap-map for the lossless non-dispersive structures with $\Omega_\mathrm{p} = 10$, showing that no first gap is expected for $\frac{r}{a} \leqslant 0.315$.

3.2. Lossy dispersive case

3.2.1. Band structure. In case of loss and dispersion in the conductivity of the conducting surface, the shape of the band structure undergoes strong deformation, as illustrated in figure 4. Here, we have assumed similar geometric parameters to the previous case study to facilitate comparisons; however, the normalized plasma frequency $\Omega_\mathrm{p} = \omega_\mathrm{p}\tau = 10$. Also, notice the difference in the normalization scheme, that is the imaginary angular frequency is normalized with the aid of relaxation time as $\nu_n = \mathrm{Im}\{\omega\tau\}$. Resemblance to the E-polarization band structure of a two-dimensional photonic crystal is no longer apparent, as the first band for low frequencies has deformed significantly. However, a striking difference from the lossless case arise from the fact that the eigenvalues are purely imaginary, when the wavenumber κ is real. Moreover, the imaginary frequency at which the first plasmonic band gap opens has moved towards lower frequencies, being this time around $\nu_n = 9.77 \times 10^{-1}$. For $\frac{r}{a} = 0.35$, the imaginary frequency band gap has a width of only $\Delta\nu_n = 1.017 \times 10^{-2}$, with a gap-ratio of just $\frac{\Delta\nu_n}{\nu_n} = 1.24\%$. Nevertheless, the gap-map has still preserved its major property, that is, we have no plasmonic band gap for $\frac{r}{a} \leqslant 0.315$. Properties and possible applications of imaginary band-structures are under further investigation.

3.2.2. Eigenmodes. Finally, taking a look at the eigenmodes of the lossy and dispersive example reveals that the presence of loss as well as dispersion has had a negligible effect on the field distribution of the eigenmodes, so the same set of modes in figures 2 and 3 is applicable with very small differences (we do not include the exact set of calculated figures for convenience). So we again have the same set of symmetries for the $\mathbf{X}_{1,2}$ and $\mathbf{M}_{1,2}$ points, which justifies the fact that the point group symmetries of these particular points are independent of all parameters but the geometrical symmetries of the original two-dimensional structure. In fact, the presence of loss and dispersion, though making the band structure remarkably distorted, has left the symmetry and even the qualitative profile of eigenmodes unchanged.

4. Conclusions

In this paper, we have presented a new formulation for the analysis of a structured conducting interface. We based our formulation on the magnetic vector-potential description of the system and employed a Green's function formalism to simplify the problem into a linear matrix eigenvalue problem. We successfully showed that it would be possible to take the full form of the dispersion into account, without any need to use specially developed numerical algorithms. This has enabled us to model the loss with full accuracy and high efficiency. The band structure and gap-map for various initial data were obtained and it was shown that an imaginary plasmonic band gap can exist. Since the structure is lossy, the loss rate could be accordingly tailored through a proper design. This might enable one to engineer the structure to be completely reflective without loss in certain parts of the frequency range, while it is otherwise lossy in the whole spectrum. The symmetries of the band structure at high symmetry points were studied and it was concluded that the structure, though having a completely different form and physics, demonstrates the same symmetry properties as a two-dimensional square-lattice photonic crystal in E-polarization.

References

[1] Raether H 1988 *Surface Plasmons on Smooth and Rough Surfaces and on Gratings* (Berlin: Springer)
[2] Ozbay E 2006 *Science* **311** 189
[3] Smalyaninov I I, Davis C C, Elliott J, Wurtz G A and Zayats A V 2005 *Phys. Rev.* B **72** 085442
[4] Maier S A, Andrews S R, Martin-Moreno L and Garcia-Vidal F J 2006 *Phys. Rev. Lett.* **97** 176805
[5] Khurgin J B 2006 *Appl. Phys. Lett.* **89** 251115
[6] Khurgin J B, Sun G and Soref R A 2007 *J. Opt. Soc. Am.* B **24** 1968

[7] Khurgin J B and Sun G 2007 *Proc. SPIE* **6638** 66380R
[8] Sun G, Khurgin J B and Soref R A 2007 *Appl. Phys. Lett.* **90** 111107
[9] Khurgin J B 2007 *Phys. Rev. Lett.* **98** 177401
[10] Pitarke J M, Silkin V M, Chulkov E V and Echenique P M 2007 *Rep. Prog. Phys.* **70** 1
[11] Wuenschell J and Kim H K 2006 *Opt. Express* **14** 10000
[12] Lan Y-C and Chern R-L 2006 *Opt. Express* **14** 11339
[13] Kajenski P J 1997 *Opt. Eng.* **36** 1537
[14] Pigeon F, Salakhutdinov I F and Tishchenko A V 2001 *J. Appl. Phys.* **90** 852
[15] Khorasani S and Rashidian B 2001 *J. Opt. A: Pure Appl. Opt.* **3** 380
[16] Khorasani S and Rashidian B 2002 *J. Opt. A: Pure Appl. Opt.* **4** 251
[17] Mehrany K, Khorasani S and Rashidian B 2003 *Semicond. Sci. Technol.* **18** 582
[18] Khorasani S and Rashidian B 2002 *Proc. SPIE* **4655** 260
[19] Mehrany K, Momeni B, Khorasani S and Rashidian B 2003 *Proc. SPIE* **4833** 535
[20] Schulkin B, Sztancsik L and Federici J F 2004 *Am. J. Phys.* **72** 1051
[21] Flindt C, Mortensen N A and Jauho A-P 2005 *Nano Lett.* **5** 2515
[22] Sakoda K 2001 *Optical Properties of Photonic Crystals* (Berlin: Springer)
[23] Shi S, Chen C and Prather D W 2005 *Appl. Phys. Lett.* **86** 043104
[24] Mohammadi A and Agio M 2006 *Opt. Express* **14** 11330
[25] Moreno E, Erni D and Hafner C 2002 *Phys. Rev.* B **65** 155120
[26] Cheng D K 1989 *Field and Wave Electromagnetics* 2nd edn (Englewood Cliffs, NJ: Prentice-Hall)